Proposing an Ultrapure Water Unit Coupled to an Existing Reverse Osmosis Desalination Plant and its Exergy Analysis

Bashayar Al Maqbali[1], Zohreh Rahimi-Ahar[2], Hasan Mousa[3], G. Reza Vakili-Nezhaad[4*]

[1]Petroleum & Chemical Engineering Department, College of Engineering, Sultan Qaboos University, Muscat 123, Oman
[2]Chemical Engineering Department, University of Isfahan, Isfahan, Iran
[3]Department of Chemical Engineering, Jordan University of Science and Technology, Irbid, Jordan
[4]Sustainable Energy Research Center (SERC), Sultan Qaboos University, Muscat 123, Oman
[1]E-mail: Vakili@squ.edu.om

Abstract

In this study, three desalination exergy analysis models including the Cerci et al. model (Model A), Drioli et al. model (Model B) and electrolyte solution model (Model C), were developed on an existing reverse osmosis (RO) desalination plant in Oman (Plant ALG). A modified ultrapure water (UPW) unit fed by Plant ALG has also been proposed (Plant A) based on the technology used in a UPW unit operated under the climate of Europe and fed by European river water (Plant B). The most suitable exergy model for characterizing the proposed UPW production plant was used. Model C was found to be the most proper model among its counterparts. It reflected the electrolytic behavior of the relevant streams and considered as the appropriate model. The major exergy destruction sites were also identified, and the exergy efficiency was calculated. The electro-de-ionization (EDI) and the RO unit were the highest exergy destructive components in Plant A.

Keywords: Reverse osmosis; ultrapure water; exergy destruction; exergy efficiency; electro-de-ionization.

1. Introduction

The relationship between water and energy production is extremely close and co-dependent [1]. The water demand is growing annually due to population growth and economic development [2]. In Oman, annually, the drinking water need is nearly 200 MCM (Million Cubic Meter), agriculture consumption is 1,600 MCM, and industrial plants consume around 130 MCM [3]. Some reports reveal that the population of Oman will be doubled in the next 20 years and will be resulting in several development projects, mainly in the water sector [4]. Several desalination plants were commissioned in different regions to meet the continuous growth of water demand and to decrease the reliance on groundwater resources [5]. Freshwater can be recovered from seawater via RO desalination technology [6]. The useful method toward more energy-efficient desalination technology is to shift from the thermal desalination plant to RO [7]. Though, the optimization of RO desalination systems are essential [8]. Exergy Analysis is an accepted and useful analytical approach for energy optimization of the desalination systems [9]. The analysis of the real thermodynamic inefficiencies in a process is valuable for enhancing an energy-intensive operation [10].

Many exergy analysis researches have been developed to identify the energetical inefficiencies. A comprehensive study was developed based on desalination exergy analysis approaches by Fitzsimons et al. [11]. The appropriateness of the Cerci et al., Drioli et al. and the ideal mixture models were a concern. The exergy destruction, specific exergy and exergy efficiency values for most approaches were similar.

The ideal mixture model resulted in meaningful differences in exergy efficiency.

Exergy analysis of an RO plant was developed using actual operation data of the plant. The primary membrane units and the throttling valves were the main exergy destructive components in the system. The overall exergy efficiency of 4.3% was calculated which could be increased to 4.9% by adding a pressure exchanger with two throttling valves [12]. A desalination plant in California including RO, nanofiltration (NF), and electrodialysis reversal (EDR) units were analyzed exergetically by Kahraman et al. [13]. The analysis showed that the motor/pump used in EDR, RO, and NF was the most to least exergy destructive components, respectively. A hybrid organic Rankine cycle (ORC) coupled with the RO system was studied by Shekari Namin et al. [14]. Low condensing pressure in proposed system caused the requirement of a large volume turbine. Using the cascade ORC or KC (Kalina cycle) as a power supply source could solve this problem. A KC cycle was coupled to an RO system to provide drinking water, power, heating and cooling [15]. The first and second condensers, flashing device, second HEX and RO systems were high exergy destructive components. The overall exergy efficiency of 38.1% was obtained in the proposed process.

A poly-generation system including RO unit, photovoltaic panels, ORC, waste heat recovery section and homogeneous charge compression ignition engine was analyzed thermodynamically by Islam et al. [16]. Coupling the Pelton turbine to the RO plant recovered 24.3% of the input power. Exergy efficiencies of system excluding and including Pelton turbine were 44.1% and 45.01%,

respectively. A waste heat-driven hybrid system containing Rankine cycle for power generation, thermochemical copper-chlorine cycle for hydrogen and RO for water production was analyzed by Ishaq et al. [17]. The maximum irreversibility took place in pump B4 and the highest exergy efficiency associated with the third compressor. Bouzayani et al. modeled three water/power-producing systems [18]. The exergy loss in the power plant was ten times more than that in the RO unit. A dynamic RO plant model was developed by Naseri et al. [19] to produce different permeate rates. Modification of the storage tank capacity minimized its temperature fluctuation, led to minimization of the exergy destruction. Ameri and Seyd Eshaghi modeled an RO plant coupled to humidification-dehumidification (HDH) system [20] by solution–diffusion method. The results indicated that the RO-HDH system increased the exergy efficiency to 20.60%, while HDH and RO exergy efficiencies were 12.66% and 0.72%, respectively.

Desalination plants that remove impurity from water are crucial in the UPW production process. The ion exchange, ultrafiltration (UF), RO, and electro-deionization processes are proposed to produce UPW [21]. A comprehensive review of the rising role of RO to satisfy the technical requirements in the UPW sector, with an emphasis on electronic industrial applications was carried out by Lee et al. [22]. Studies on synergetic effects with other purification technologies were proposed as an in urgent demand. Zhan et al. [23] proposed a RO unit using the modified fouling index to support the stable operation of UPW plant applications. An intimate correlation between the modified fouling index and RO performance was revealed via electrochemical deionization concentrate. Jin et al. [24] used ultraviolet radiation to RO pretreatment to produce UPW. It was also revealed that the use of UPW is essential in increasing the energy efficiency of the cogeneration plants [25].

Three exergy analysis approaches using real operational data were applied to characterize ALG Plant (the main desalination plant in Oman) and the best approach could be selected. A modified UPW unit fed by ALG Plant was designed (Plant A) based on the technology used in an UPW unit operated under the climate of Europe and fed by European river water (Plant B). Exergy analysis of an integrated RO-UPW unit could provide an energy-efficient plant that has not been paid attention. Plant A was proposed to produce high-purity water which is useful in many advanced high-tech applications.

2. Methodology

This work investigates an existing RO plant coupled to a UPW unit exergetically. The exergy analysis process is summarized as follows:

1- Three exergy analysis models on an existing RO desalination plant are performed based on the real operation conditions. Temperature, pressure, salinity (See Table 1) are directly used in exergy equations as described in Section 2.5.

2- The best exergy analysis model is selected via comparing the models concept as well as the physical and chemical exergy contents.

3- A modified UPW unit fed by RO plant is proposed (Plant A) based on the technology used in a UPW unit operated under the climate of Europe and fed by European river water (Plant B).

4- The most suitable exergy model can be selected for characterizing RO-UPW production plant. The major exergy

destruction sites are identified followed by exergy efficiency calculations.

Proposing a UPW plant with high quality water production, introducing the most exergy destructive components in proposed plant and some recommendations for exergy efficiency improvement can pave the way for future real research in this field.

2.1 Plant description

The plant is located in Muscat and is operated based on RO technology. It is capable of producing 24,000 m3 of potable water per day to supply the domestic requirements. The flow diagram of the proposed system is illustrated in Figure 1.

2.2 Plant description

The seawater with a salinity of 38,321 ppm at a flow rate of 2,500 m^3/h was pumped by a low-pressure pump (stream 0). The incoming seawater was separated at the end into two streams. The brine with a salinity of 63,623 ppm was disposed to the sea at a flow rate of 1,500 m^3/h (stream 13) and permeate with a salinity of less than 321 ppm was pumped to the product tank at a flow rate of 1,000 m^3/h (stream 7).

2.3 Plant operating condition

Due to the high salinity of the incoming seawater to the plant, the proposed process was pretreated with multimedia filtration (MMF) followed by fine filtration (cartridge filter) and finally, RO process was used for removal of salts from the seawater, to make it suitable for human use. The plant was operated at a constant temperature of 40℃. The pressure of the incoming seawater increased from 100 kPa at the inlet to 340 kPa before it entered the MMF. It was increased up to 689 kPa before it entered the cartridge filter. A high-pressure pump increased the pressure of the incoming seawater to 6,080 kPa before introducing the seawater to the RO unit. The brine left the RO unit at 5,400 kPa. The pressure of the brine was reduced using three throttling valves to 200 kPa before disposing the brine to the sea. Permeate was left the RO unit at 100 kPa and was pumped to the chamber blending at 290 kPa. The operating conditions and the quality of each stream at each process stage are summarized in Table 1.

Table 1. Plant operating conditions.

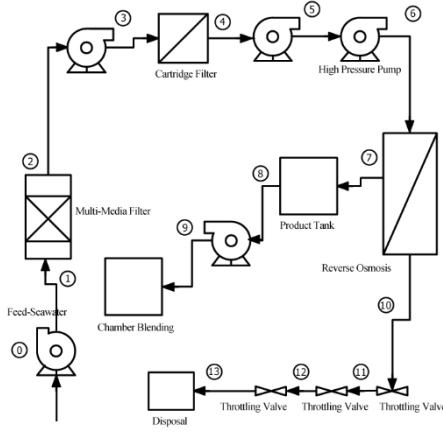| Process Stream	P (kPa)	T (°C)	Total dissolved solid (TDS) (mg/L)	Volumetric Flowrate (m^3/h)
0	100	40.0	38,321	2,500
1	340	40.0	38,322	2,500
2	340	40.0	38,323	2,500
3	689	40.0	38,324	2,500
4	689	40.0	38,325	2,500
5	1,000	40.0	38,326	2,500
6	6,080	40.0	38,327	2,500
7	100	40.0	321	1,000
8	100	40.0	322	1,000
9	290	40.0	323	1,000
10	5,400	40.0	63,622	1,500
11	2,700	40.0	63,623	1,500
12	1,200	40.0	63,624	1,500
13	200	40.0	63,625	1,500

Figure 1. The flow diagram of the proposed RO desalination plant

2.4 Thermodynamic properties of seawater

In proposed process, the operating pressure was upper than 6 MPa. An accurate method was used to estimate the pressure effect on the seawater properties. The pressure-dependent correlation developed by Nayar et al. [26] was used for seawater properties calculation.

2.5 Desalination plant exergy models
2.5.1 Cerci et al. model (Model A)

In the Cerci et al. model (Model A), the system is treated as an ideal mixture of Sodium Chloride (NaCl) and water. The salinity of 3.5% is considered in Model A. Total exergy (chemical and physical) of the Cerci et al. model is calculated as [26]:

$$\dot{E} = \dot{m}\left[[(w_s h_s) + (w_w h_w)] - [(w_s h_s) + (w_w h_w)]_0 - T_0[[w_s s_s + w_w s_w] - [w_s s_s + w_w s_w]_0] + T_0[[R_{im}(x_s ln x_s + x_w ln x_w)] - [R_{im}(x_s ln x_s + x_w ln x_w)]_0]\right] \tag{1}$$

where water and salt mole fractions are calculated using Eqs. 2 and 3, respectively [1]:

$$x_w = \frac{MW_w}{MW_s\left[\frac{1}{w_s}-1\right]+MW_w} \tag{2}$$

$$x_s = \frac{MW_s}{MW_w\left[\frac{1}{w_w}-1\right]+MW_s} \tag{3}$$

NaCl is considered as an incompressible solid in the Cerci et al. model [12]. The specific entropy and specific enthalpy of the NaCl are 0.0172 kJ/kg.K and 33.472 kJ/kg, respectively. The specific enthalpy of the water is calculated at different stages using Eq. 4.

$$h_{sw}(t,S,P) = h_{sw}(t,S,P_0) + (P - P_0)(m_1 + m_2 t + m_3 t^2 + m_4 t^3 + s(m_{5+}m_6 t + m_7 t^2 + n_8 t^3)) \tag{4}$$

Where,

$$h_{sw}(t,S,P_0) = h_w(t) - S_{\frac{Kg}{Kg}}(n_1 + n_2 S_{kg/kg} + n_3 S_{kg/kg}^2 + n_4 S_{kg/kg}^3 + n_5 t + n_6 t^2 + n_7 t^3 + n_8 S_{kg/kg} t + n_9 S_{kg/kg}^2 t + n_{10} S_{kg/kg} t^2) \tag{5}$$

where m₁-m₈ and n₁-n₁₀ are introduced in section A.3.

$$h_w = 141.355 + 4202.07t - 0.535t^2 + 0.004t^3 \tag{6}$$

The specific entropy of the water is calculated as:

$$s_{sw}(t,S,P) = s_{sw}(t,S,P_0) + (P - P_0)(m_1 + m_2 t + m_3 t^2 + m_4 t^3 + S(m_5 + m_6 t + m_7 t^2 + m_8 t^3)) \tag{7}$$

where

$$s_{sw}(t,S,P_0) = s_w(t) - S_{\frac{kg}{kg}}\left(n_1 + n_2 S_{\frac{kg}{kg}} + n_3 S_{kg/kg}^2 + n_4 S_{kg/kg}^3 + n_5 t + n_6 t^2 + n_7 t^3 + n_8 S_{\frac{kg}{kg}} t + n_9 S_{kg/kg}^2 t + n_{10} S_{kg/kg} t^2\right) \tag{8}$$

where m_i and n_i are presented in Appendix A.3. The specific entropy of the salt is calculated as:

$$s_s = 0.1543 + 15.383t + 2.996 \times 10^{-2}t^2 + 8.193 \times 10^{-5}t^3 - 1.370 \times 10^{-7}t^4 \tag{9}$$

2.5.2 Drioli et al. model (Model B)

In Drioli et al. model, the system is treated as an ideal aqueous solution of ions (Cl⁻, Na⁺, SO4⁻², K⁺). The dead state is defined as pure water at atmospheric pressure and ambient temperature. The total exergy rate is a summation of thermal, pressure and chemical exergy rates as:

$$\dot{E} = \dot{E}^{Th} + \dot{E}^P + \dot{E}^{Ch} \tag{10}$$

where the thermal, pressure and chemical exergy rate terms are calculated as:

$$\dot{E}^{Th} = \dot{m}c\,(T - T_0) \tag{10.1}$$

$$\dot{E}^P = \dot{m}\left[\frac{P - P_0}{\rho}\right] \tag{10.2}$$

$$\dot{E}^{Ch} = -\dot{m}\,N_w R T_0 \ln x_w \tag{10.3}$$

where

$$N_w = \frac{(1 - \sum \frac{C_i}{\rho})}{MW_w} \qquad (11)$$

$$x_w = \frac{N_w}{\left[N_w + \sum \left(\frac{\beta_i C_i}{\rho MW_i}\right)\right]} \qquad (12)$$

2.5.3 Electrolyte solution exergy analysis model (Model C)

In the electrolyte solution approach, the system is treated as a non-ideal ionic solution [11]. The activity of species is calculated as:

$$a_i = m_i \gamma_{H_i} \qquad (13)$$

The activity of an electrolyte solution including seawater requires Pitzer equations [27]. For the single electrolyte of anion X and cation M, the activity coefficient is calculated as:

$$ln\,\gamma_{\pm} = -|z_m z_X| A^{\phi} \left[\frac{2}{b} ln\,ln\left(1 + b\sqrt{I}\right) + \right. \qquad (14)$$

$$\left. \frac{\sqrt{I}}{1+b\sqrt{I}}\right] + m \frac{2v_M v_X}{v} \left\{2\beta_{MX}^{(0)} + \frac{2\beta_{MX}^{(1)}}{\alpha^2 I}\left[1 - \left(1 + \right.\right.\right.$$

$$\left.\left.\left. \alpha\sqrt{I} - \frac{\alpha^2 I}{2}\right)e^{-\alpha^2 I}\right]\right\} + \frac{3m^2}{2}\left[\frac{2v_M v_X^{\frac{3}{2}}}{v} C_{MX}^{\emptyset}\right]$$

where, A^{ϕ} is 0.3882, b and α are constant parameters. For a 1–1 electrolyte b and α are 1.2 and 2, respectively. $C_{MX}^{\emptyset}$, $\beta_{MX}^{(0)}$ and $\beta_{MX}^{(1)}$ are empirical parameters and their values are 0.002, 0.0714 and 0.2723, respectively. The solvent activity is calculated by the following equation.

$$ln\,a_w = -\emptyset \frac{vm}{55.51} \qquad (15)$$

where, $\emptyset$ is the osmotic coefficient and is calculated as:

$$\emptyset - 1 = -|z_m z_X| A^{\phi} \frac{\sqrt{I}}{1+b\sqrt{I}} + m \frac{2v_M v_X}{v}\left[\beta_{MX}^{(0)} + \right. \qquad (16)$$

$$\left. \beta_{MX}^{(1)} e^{-\alpha^2 I}\right] + m^2 \left[\frac{2(v_M v_X)^{\frac{3}{2}}}{v} C_{MX}^{\emptyset}\right]$$

The mole fraction of salt and water is calculated using Eqs.17 and 18, respectively.

$$x_s = \frac{\beta N_s}{\beta N_s + N_w} \qquad (17)$$

$$x_w = \frac{N_s}{\beta N_s + N_w} \qquad (18)$$

3. Results and discussion

Water quality parameters including chemical and physical properties were tested based on the desired specifications. Parameters that were frequently sampled for water quality include temperature, TDS, density, pressure and composition. The exergy analysis was performed based on real data obtained from the experimented plant.

3.1 Exergy contents

As the process was isothermal, the physical exergy was achieved due to the difference in the dead state and the pressure of streams. Specific chemical and physical exergy contents calculated using three models are tabulated in Table 2.

Table 2. Specific chemical and physical exergy contents calculated using Models A, B and C.

Stream	e_{ph} Model A	e_{ph} Model B	e_{ph} Model C	e_{ch} Model A	e_{ch} Model B	e_{ch} Model C
0	0.0000	0.0000	0.0000	0.0000	3.3052	0.0000
1	0.2320	0.2351	0.2351	0.0000	3.3048	0.0000
2	0.2320	0.2351	0.2351	0.0000	3.3048	0.0000
3	0.5694	0.5770	0.5770	0.0000	3.3042	0.0000
4	0.5694	0.5770	0.5770	0.0000	3.3042	0.0000
5	0.8701	0.8817	0.8817	0.0000	3.3037	0.0000
6	5.7814	5.8581	5.8581	0.0000	3.3044	0.0000
7	0.0000	0.0000	0.0000	1.6807	0.0288	3.1349
8	0.0000	0.0000	0.0000	1.6805	0.0289	3.1345
9	0.1837	0.1861	0.1861	1.6803	0.0290	3.1341
10	5.1239	5.1920	5.1920	0.3354	5.3440	0.6173
11	2.5136	2.5470	2.5470	0.3354	5.3386	0.6174
12	1.0635	1.0776	1.0776	0.3355	5.3419	0.6174
13	0.0967	0.0980	0.0980	0.3355	5.3452	0.6175

As the process was isothermal, the physical exergy resulted due to the difference between the process pressure and the dead state pressure. For Models B and C, the similar equations were used to calculate the physical exergy rate; hence, for both models the physical exergy rates were the same. However, there was little difference in the specific physical exergy calculated using Model A and the specific physical exergy calculated using Models B and C. The difference between the specific physical exergy obtained by Model A and the specific physical exergy obtained using Models B and C did not exceed 1.3%; hence, no further investigation was required for the physical exergy term. The chemical exergy rates calculated using Models A and B were not comparable due to different salinity dead states. For Models A and C, the dead state of the solution was defined as the salinity of the incoming water; accordingly, the chemical exergy was zero in streams 0-6. It was found that Model A was an unsuitable approach as it considered an ionic solution as a mixture of water and solid salt. Accordingly, NaCl was treated as a single component in water. Furthermore, the coupling of the chemical and physical exergy equations did not provide a comprehensive understanding of chemical and physical exergy contents. The chemical exergy rates obtained using Model B were quite different from than that of the other models due to the different dead states. A negligible change in brine composition made the use of Model B an improper method for the exergy analysis of a desalination unit. Model C treated the system as a non-ideal mixture of water and NaCl and the mole fraction calculation was based on ionization of NaCl to Na^+ and Cl^-. It means even a low change in

concentration was considered. The exergy model could clarify the electrolytic behavior of the streams. On this basis, Model C was the proper model for the exergy analysis of the proposed UPW plant. In this research, seawater is assumed as a dilute solution with a typical salinity mass fraction of 3.8% [26].
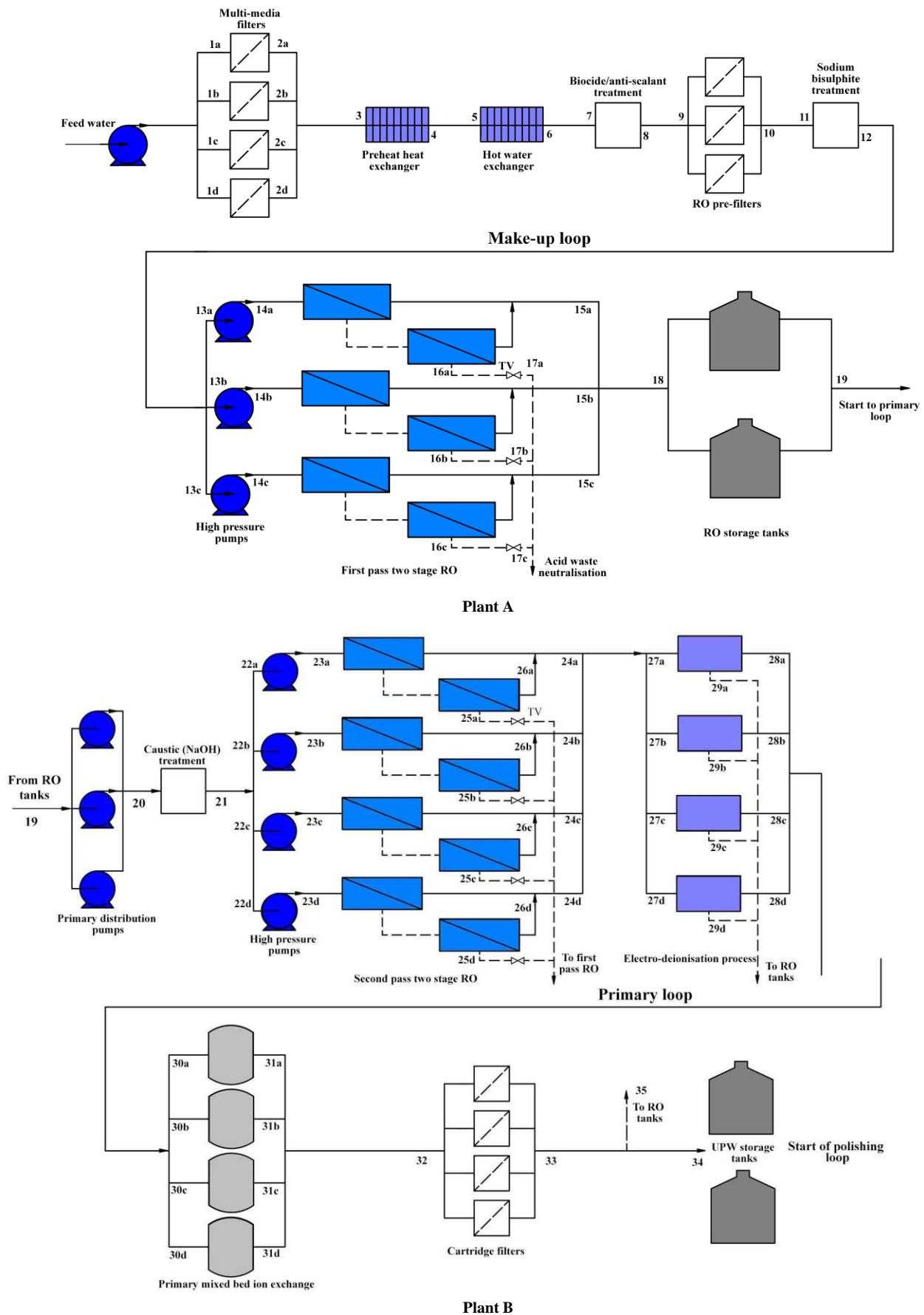

Figure 2. The process flow diagrams of the makeup and primary loops in Plants A and B.

3.2 Ultrapure water production plant analysis

Thermodynamic analysis using Model C applied for a UPW production plant operated under the climate of Oman and fed by the product of ALG Plant (Plant A). Plant A was designed using the UPW technology applied in Europe. The results were compared with the same UPW production plant operated under the climate of Europe and fed by European river water (Plant B). The process flow diagrams of the makeup and primary loops in Plants A and B are shown in Figure 2. The plant consisted of three sections; makeup, primary and polishing loops. However, in this research, only the makeup and the primary loops were analyzed. This was due to a high difference in the concentration of the incoming water. The make-up and primary loops included various levels of filtration from MMF, first and second-pass RO, ion exchange, and EDI unit. The real data used to conduct the thermodynamic analysis is detailed in Table A.2. The defined dead states of UPW production Plants A and B are tabulated in Table 3. Plants A and B differed in the temperature and the incoming water quality (TDS) due to the different climate and sources of the feedstock under which these plants were operated.

Table 3. Dead states of plants A and B.

Dead state	Parameters	Plant A	Plant B
Physical dead state	Temperature (℃)	40	16
	Pressure (bar)	1	1
Chemical dead state	TDS (ppm)	314	135

3.2.1 Exergy rates

Chemical, physical and overall exergy rates were calculated using Model C and the results for each process stream are given in Table A.3

The physical exergy for the most process stages in Plants A and B was negligible. However, there was a substantial difference in the chemical exergy between Plants A and B due to their different water properties. The high salinity of the incoming water in Plant A resulted in high chemical exergy in most of the process stages. For all process streams, physical exergy was the major source of the total exergy. The total exergy rates exceed 100 kW for both Plants A and B, and represented in Figures 3 and 4, respectively.

For both Plants A and B, the highest exergy rates were at the inlets of the hot water HEXs (Stream 5) showing the values of 640.11 kW and 686.068 kW, respectively. The outlet of the hot water HEXs (Stream 6) and the inlet of the pre-heat HEXs (Stream 3) had the next rankings in the exergy rates. Table 4 shows the first three highest exergy rates recorded for Plants A and B.

Table 4. First three highest exergy rates recorded for Plants A and B.

Process	Process Stream	Total Exergy (kW)	
		Plant A	Plant B
Pre-heat HEX	Stream 3 (Heating water-inlet)	115.98	119.455
Hot water HEX	Stream 5 (Heating water-inlet)	640.11	686.068
	Stream 6 (Heating water-outlet)	458.16	524.169

For Plant A, at the inlet of the hot water HEX, the exergy rate was higher than that of the pre-heat HEX, due to its higher temperature difference with the dead state.
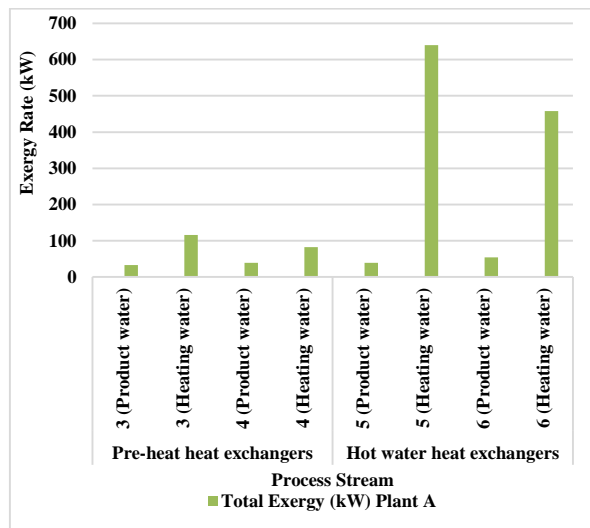

Figure 3. Total exergy rate exceeds 100 kW for UPW production Plant A.
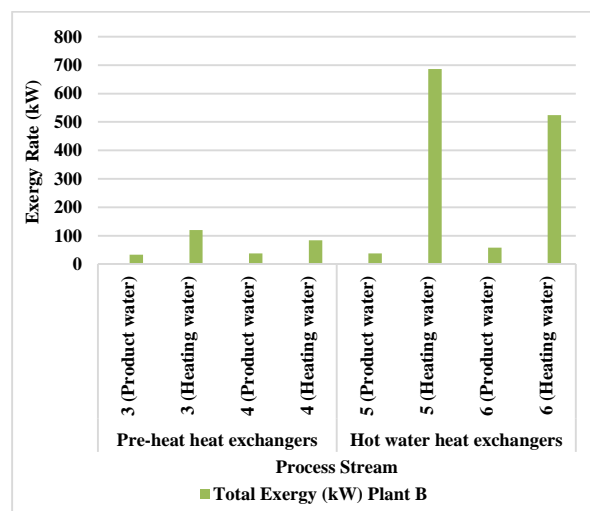
Figure 4. Total exergy rate exceeds 100 kW for UPW production Plant B.

3.2.2 Exergy destruction rates

Exergy was delivered to the UPW plant by feed water at certain values of concentration, pressure, temperature, and flow rate. The exergy was added by electrical energy input to the pumps and the EDI unit. Owing to temperature difference, throttling process, mixing and separation operations, exergy was destroyed.

The exergy destruction rates increasing due to irreversibility in the primary and make-up loops of UPW plant A showed that the key source of exergy destruction was the hot water HEX. This was supported by the results of the exergy destruction of Plant B, which are presented in Table 5.

The constant concentration during the process conducted by Plants A and B did not cause exergy destruction by chemical exergy. Hence, the differences in exergy destruction were caused by the differences in physical exergy.

The top exergy destructive components with 95% contribution in total exergy destruction within Plant A, are shown in Figure 5.

The hot water HEX, first- and second-pass RO high-pressure pumps, EDI, second and first-pass RO recorded the highest exergy destruction values. In a hot water HEX, heat transferred due to a large temperature difference; hence, an

excessive heat transfer area of finned type should be recommended. However, economical optimization is proposed for selecting the area of such an exchanger. For the first and second-pass RO high-pressure pumps, the exergy destructed due to the pressure exergy. The pressure increase from 4.7 bar to about 10 bar and from 4.3 bar to 20.9 bar for first and second-pass RO high-pressure pumps, respectively, caused exergy destruction. Coupling the variable speed drive or motor managers to pumps can be recommended to enhance the pump exergy efficiency. In the first- and second-pass RO, the temperature was constant while the increase in the pressure resulted in exergy destruction. For improving the RO process, reducing the pressure drop across the membrane can be proposed to decrease the operating pressure required to achieve acceptable permeate fluxes.

Table 5. The exergy destruction of Plants A and B.

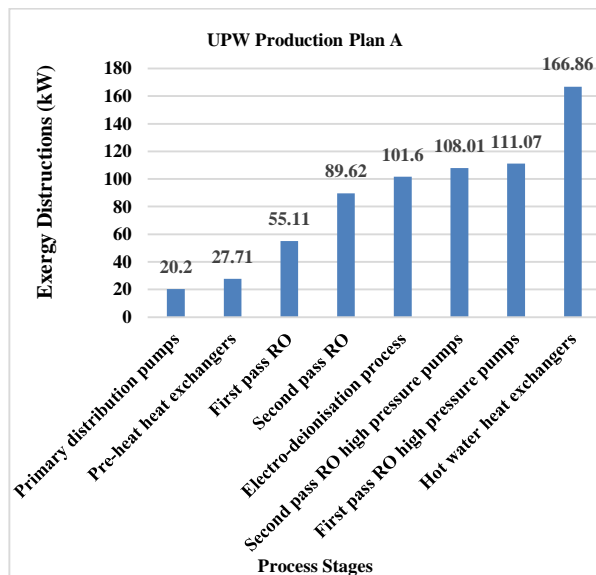| Process	Process Stream	Exergy Destructions (kW)	
		Plant A	Plant B
MMF	b	0.45	0.50
	c	0.43	0.40
	d	0.41	0.40
Pre-heat HEXs		27.71	30.90
Hot water HEXs		166.86	140.60
Biocide/anti-scalant treatment		0.60	0.60
RO pre-filters		2.60	2.60
Sodium bisulfite treatment		0.60	0.60
First-pass RO high-pressure pumps	a	55.45	55.40
	c	55.62	55.60
First-pass RO	a	31.26	31.26
	c	23.85	23.85
Throttling valves	a	8.00	8.00
	c	4.34	4.30
RO tank		1.80	1.78
Primary distribution pumps		20.20	20.18
Caustic treatment		0.60	0.60
First-pass RO high-pressure pumps	b	34.65	34.70
	c	38.18	38.20
	d	35.18	35.20
Second-pass RO	b	30.35	30.26
	c	30.04	29.96
	d	29.23	29.16
Throttling valves	b	4.70	4.70
	c	5.28	5.20
	d	4.97	5.00
EDI process	b	38.70	38.78
	c	32.00	31.96
	d	30.90	30.87
Primary mixed bed ion exchange	b	1.14	1.07
	c	1.14	1.07
	d	1.14	1.07
One-micron cartridge filters		0.13	0.54

Figure 5. Top exergy destructive components in Plant A.

3.2.3 Exergy efficiency

The exergy efficiency was calculated for the first six highest exergy destructive component. The rational exergy efficiency approach was used for the exergy efficiency calculation [28,29]. The rational exergy efficiency was calculated as:

$$Efficiency_{ex} = \frac{\dot{E}_{Desired\ output}}{\dot{E}_{used}} \qquad (19)$$

The exergy efficiencies of the process streams are tabulated in Table 6.

The exergy destruction rate of the hot water HEX (166.9 kW) was higher than that of the pre-heat HEX (27.7 kW), leading to the lower exergy efficiency of the hot water HEX compared to the pre-heat HEX. To bring the exergy efficiency of the hot water HEX up to the pre-heat HEX, 7 kW could be saved. If the plant consumed 7.94 USD/kWh, the annual saving could be 2548.32 USD.

For the first-pass RO pumps, the exergy efficiency of modules (a) and (c) was 35.5% and 25.8%, respectively. The pressure in the module (c) increased from 4.7 bar to 10 bar by consuming 75 kW. While, by increasing the pressure of module (a) from 4.7 bar to about 13 bar, 86 kW was consumed. To bring the exergy efficiency of module (c) up to module (a), 3.9 kW was saved. If the plant consumed 3.9 USD/kWh, the annual saving would be 1335.21 USD.

The exergy efficiency of the RO process was significantly greater than the EDI process. The exergy efficiency of the RO process was affected by the energy consumption of the pump while the EDI exergy efficiency was affected by the energy consumption of the brine recycling pumps and rectifiers, which lowered the exergy efficiency of the EDI process, compared to the RO process.

The exergy efficiency of the first-pass RO process was ten times higher than that of the second-pass RO process. The second-pass RO modules were similar in terms of exergy efficiency. However, the exergy efficiency of module (c) in the first-pass RO was 32% more than module (a), due to different TDS and pressure drop by two modules.

The exergy efficiency of EDI module (b) was lower than modules (c) and (d). The higher energy drawn by the module (b) rectifiers caused this difference in exergy efficiency. The

lower exergy efficiency values of the EDI and the second-pass RO processes should be noted. As the purity of the water increased, the change in the chemical exergy rate decreased, lowering the exergy efficiency of the RO and EDI processes.

Table 6. The exergy efficiency of the process streams.

Component	Process stream	Exergy efficiency%
Hot water HEX		8.292
First RO high-pressure pumps	a	35.519
	c	25.835
Second RO high-pressure pumps	b	51.880
	c	50.418
	d	51.781
EDI	b	0.013
	c	0.017
	d	0.018
Second-pass RO	b	0.267
	c	0.254
	d	0.269
First-pass RO	a	3.663
	c	4.841
Pre-heat HEX		18.001
Primary distribution pumps		43.473

3. Conclusion

Exergy analysis has been made on an existing RO desalination plant (ALG) in Oman to find out the potential of energy-saving options. A modified ultrapure water (UPW) unit fed by ALG Plant was proposed [Plant A] based on the technology used in a UPW unit operated under the climate of Europe and fed by European river water [Plant B]. Three desalination exergy analysis models including the Cerci model (Model A), Drioli model (Model B) and electrolyte solution model (Model C), were developed on ALG Plant. Model C well reflected the electrolytic behavior of the process streams.

The exergy rate calculations showed the highest exergy rates were related to the inlet of the hot water heat exchangers (640.11 kW for Plant A and 686.068 kW for Plant B), followed by the outlet of the hot water heat exchangers (458.16 kW for Plant A and 524.169 kW for Plant B) and the inlet of the pre-heat heat exchangers (115.98 kW for Plant A and 119.455 kW for Plant B).

Second RO high-pressure pumps, primary distribution pumps and first RO high pressure pumps were the exergy efficient components while EDI, second-pass RO, first-pass RO, hot water HEX and pre-heat HEX with exergy efficiency of less than 20% were the most exergy destructive components.

Application of an HEX with higher contact area by consideration of economical point view, coupling the variable speed drive or motor managers to pumps and reducing the pressure drop across the membrane can be recommended to enhance the HEX, pumps and RO unit exergy efficiency, respectively.

Acknowledgements:

Nomenclature

Roman symbol

a	Activity
$A^{\emptyset}$	Pitzer model parameter
b	Pitzer model parameter
B	Debye–Huckel parameter
c	Concentration, kg/L
cp	Specific heat capacity at constant volume, kJ/kg.K
c_v	Specific heat capacity at constant volume, kJ/kg·K
$C^{\emptyset}$	Pitzer parameter
h	Specific enthalpy, kJ/kg
$\dot{E}$	Exergy rate, kW
I	Ionic strength of a solution, moles of solute/kg of solvent
$\dot{m}$	Mass flowrate, kg/s
m	molality, mole/kg
MW	Molecular weight, kg/kmol
N	Moles number
P	Pressure at the process stage under consideration, kPa
R	Universal gas constant, kJ/kmol·K
s	Specific entropy, kJ/kg.K
S	Salinity, kg/kg
t	Celsius temperature, ℃
T	Temperature, K
w	Mass fraction, kg of solvent or solute/kg of solution
x	Mole fraction, mole of solvent or solute/mole of solution
z	Valence of the ions

Greek

α	Parameter for the Debye–Huckel model
β	Number of ions of solute generated on dissociation
$\beta_{MX}^{(n)}$	Pitzer equation parameter
ρ	Density, kg/m³
$\emptyset$	Osmotic coefficient
v	Number of ions generated on the dissociation of the electrolyte
$\gamma_{\pm}$	Activity coefficient

Superscript

Ch	Chemical
P	Pressure
Th	Thermal

Subscript

0	Dead state
i	Species
H	Henry
M	Denotes to the cation
s	Salt
$soln$	Solution
w	Water
X	Denotes to the anion

Abbreviation

EDR	Electrodialysis reversal
EDI	Electro-deionization
HDH	Humidification-dehumidification

HEX   Heat exchanger
KC   Kalina cycle
MCM   Million cubic meter
MMF   Multi-media filter
NF   Nanofiltration
ORC   Organic Rankine cycle
RO   Reverse osmosis
UPW   Ultrapure water

Appendix

A.1 Water analysis

Water analysis from sampled water clarified the compositions, which are tabulated in Table A

A.2 Constants of specific enthalpy and entropy of the water

The constants of specific enthalpy of the water is evaluated by:

m_1=996.7767, m_2=-3.2406, m_3=0.0127, m_4=-4.7723×10^{-5},

m_5=-1.1748, m_6=0.01169, m_7=-2.6185×10^{-5},

m_8=7.0661×10^{-8}

n_1=-2.34825×10^4, n_2=3.15183×10^5, n_3=2.80269×10^6,

n_4=-1.44606×10^7, n_5=7.82607×10^3, n_6=-4.41733×10^1,

n_7=2.1394×10^{-1}, n_8=-1.99108×10^4, n_9=2.77846×10^4,

n_{10}=9.72801×10^1

The constants of specific entropy of the water is evaluated by:

m_1==-4.4786×10^{-3}, m_2=-1.1654×10^{-2}, m_3=6.1154×10^{-5},

m_4=-2.0696×10^{-7}, m_5=-1.5531×10^{-3}, m_6=4.0054×10^{-5},

m_7=-1.4193×10^{-7}, m_8=3.3142×10^{-10}

n_1=-4.231×10^2, n_2=1.463×10^4, n_3=-9.880×10^4,

n_4=3.095×10^5, n_5=2.562×10^1, n_6=-1.443×10^{-1},

n_7=5.879×10^{-4}, n_8=-6.111×10^1, n_9=8.041×10^1,

n_{10}=3.035×10^{-1}

A.3 The process data of Plants A and B

The real data used to conduct the thermodynamic analysis is detailed in Table A.2

A.4 The calculated physical, chemical and total exergy rates using Model C at each process stream

Chemical, physical and overall exergy rates were calculated using Model C and the results for each process stream are given in Table A.3.

Table A.1. Compositions (mg/L) of experimented water.

Process Stream	Ca	Mg	Na	K	CO_3	HCO_3	SO_4	Cl	NO_3	B	SiO_2	CO_2
0	473	1400	11713	493	40	103	2861	21223	7	5	3	0
1	473	1400	11713	493	40	103	2861	21223	7	5	3	0
2	473	1400	11713	493	40	103	2861	21223	7	5	3	0
3	473	1400	11713	493	40	103	2861	21223	7	5	3	0
4	473	1400	11713	493	40	103	2861	21223	7	5	3	0
5	473	1400	11713	493	40	103	2861	21223	7	5	3	0
6	473	1400	11713	493	40	103	2861	21223	7	5	3	0
7	1	3	113	6	0	1	6	183	0	0	0	0
8	1	3	113	6	0	1	6	183	0	0	0	0
9	1	3	113	6	0	1	6	183	0	0	0	0
10	788	2332	19454	818	29	155	4764	35249	11	7	5	0
11	788	2332	19454	818	29	155	4764	35249	11	7	5	0
12	788	2332	19454	818	29	155	4764	35249	11	7	5	0
13	788	2332	19454	818	29	155	4764	35249	11	7	5	0

Table A.2. The process data of Plants A and B.

Process	Process stream	Q (m³/h)	T (°C) Plant A	T (°C) Plant B	P (bar)	TDS (ppm) Plant A	TDS (ppm) Plant B	Power (kW)
MMF	1b	81.4	40	16	6.2	314.00	318.01	
	1c	78.2	40	16	6.2	314.00	318.01	
	1d	74.6	40	16	6.2	314.00	318.01	
	2b	81.4	40	16	6	314.00	318.01	
	2c	78.2	40	16	6	314.00	318.01	
	2d	74.6	40	16	6	314.00	318.01	
Pre-heat HEXs	3 (Product water)	234.2	40	16	6	314.00	318.01	
	3 (Heating water)	507	46	22	6.9	314.00	318.01	
	4 (Product water)	234.2	45	21	5.3	314.00	318.01	
	4 (Heating water)	507	44	20	5.8	314.00	318.01	
Hot water HEXs	5 (Product water)	234.2	45	21	5.3	314.00	318.01	
	5 (Heating water)	78	112	88	7.3	314.00	318.01	
	6 (Product water)	234.2	48	24	5.1	314.00	318.01	
	6 (Heating water)	78	100	76	6.2	314.00	318.01	
Biocide/anti-scalant treatment	7	234.2	48	24	5.1	314.00	318.01	0.6
	8	234.2	48	24	5.1	314.00	318.01	
RO pre-filters	9	234.2	48	24	5.1	314.00	318.01	
	10	234.2	48	24	4.7	314.00	318.01	
Sodium bisulfite treatment	11	234.2	48	24	4.7	314.00	318.01	0.6
	12	234.2	48	24	4.7	314.00	318.01	
First-pass RO high-pressure pumps	13a	130.9	48	24	4.7	297.67	301.47	86
	13c	131.6	48	24	4.7	297.67	301.47	75
	14a	130.9	48	24	13.1	297.67	301.47	
	14c	131.6	48	24	10	297.67	301.47	
First-pass RO	15a	95.8	48	24	2.2	5.42	5.49	
	15c	97.6	48	24	2.2	7.56	7.65	
	16a	35.1	48	24	10.2	1095.34	1109.33	
	16c	34	48	24	6.6	1130.45	1144.89	
	17a	35.1	48	24	2	1095.34	1109.33	
	17c	34	48	24	2	1130.45	1144.89	
RO tank inlet	18	242.9	48	24	2	6.26	6.34	
RO tank outlet (Pumps inlet)	19	242.9	48	24	2	6.26	6.34	35.7
Primary pumps out (Caustic inlet)	20	242.9	48	24	4.3	6.26	6.34	0.6

Caustic treatment outlet	21	242.9	48	24	4.3	22.82	23.11	
Second-pass RO high-pressure pumps	22b	81	48	24	4.3	22.82	23.11	72
	22c	79.4	48	24	4.3	22.82	23.11	77
	22d	82.5	48	24	4.3	22.82	23.11	73
	23b	81	48	24	20.9	22.82	23.11	
	23c	79.4	48	24	21.9	22.82	23.11	
	23d	82.5	48	24	20.8	22.82	23.11	
Second-pass RO	24b	70.8	48	24	5.8	1.30	1.31	
	24c	68.6	48	24	6.5	1.30	1.31	
	24d	71.1	48	24	6.5	1.30	1.31	
	25b	10.2	48	24	18.6	172.19	174.39	
	25c	10.8	48	24	19.6	159.52	161.56	
	25d	11.4	48	24	17.7	157.08	159.08	
	26b	10.2	48	24	2	172.19	174.39	
	26c	10.8	48	24	2	159.52	161.56	
	26d	11.4	48	24	2	157.08	159.08	
EDI	27b	72.8	48	24	6.2	1.30	1.31	33.9
	27c	70.1	48	24	6.1	1.30	1.31	27.6
	27d	70	48	24	6.2	1.30	1.31	26.3
	28b	65.1	48	24	4	0.05	0.05	
	28c	65.2	48	24	4	0.05	0.05	
	28d	64.8	48	24	4	0.05	0.05	
	29b	7.7	48	24	2	11.60	11.75	
	29c	4.9	48	24	2	17.63	17.86	
	29d	5.2	48	24	2	16.56	16.77	
Primary mixed bed ion exchange	30b	66.3	48	24	3.6	0.05	0.05	
	30c	63.4	48	24	3.6	0.05	0.05	
	30d	64.8	48	24	3.6	0.05	0.05	
	31b	66.3	48	24	3	0.04	0.04	
	31c	63.4	48	24	3	0.04	0.04	
	31d	63.8	48	24	3	0.04	0.04	
One-micron cartridge filters	32	194.5	48	24	2.9	0.04	0.04	
	33	194.5	48	24	2.8	0.04	0.04	
UPW tank inlet	34	162.8	48	24	2.8	0.04	0.04	
Diverted flow to RO tanks	35	31.7	48	24	2.8	0.04	0.04	

Table A.3. The calculated physical, chemical and total exergy rates using Model C at each process stream

Process	Process stream	Physical exergy (kW)		Chemical exergy (kW)		Overall exergy (kW)	
		Plant A	Plant B	Plant A	Plant B	Plant A	Plant B
MMF	1b	11.728	11.800	0.000	0.074	11.73	11.874
	1c	11.267	11.300	0.000	0.071	11.27	11.371
	1d	10.748	10.800	0.000	0.067	10.75	10.867
	2b	11.276	11.300	0.000	0.074	11.28	11.374
	2c	10.832	10.900	0.000	0.071	10.83	10.971
	2d	10.334	10.400	0.000	0.067	10.33	10.467
Pre-heat HEXs	3 (Product water)	32.442	32.500	0.000	0.212	32.44	32.712
	3 (Heating water)	115.982	119.000	0.000	0.455	115.98	119.455
	4 (Product water)	38.525	36.900	0.000	0.210	38.52	37.110
	4 (Heating water)	82.188	83.700	0.000	0.455	82.19	84.155
Hot water HEXs	5 (Product water)	38.525	36.900	0.000	0.211	38.52	37.111
	5 (Heating water)	640.113	686.000	0.000	0.068	640.11	686.068
	6 (Product water)	53.613	58.200	0.000	0.210	53.61	58.410
	6 (Heating water)	458.162	524.100	0.000	0.069	458.16	524.169
Biocide/anti-scalant treatment	7	53.613	58.200	0.000	0.209	53.61	58.409
	8	53.613	58.200	0.000	0.209	53.61	58.409
RO pre-filters	9	53.613	58.200	0.000	0.209	53.61	58.409
	10	51.010	55.600	0.000	0.209	51.01	55.809
Sodium bisulfite treatment	11	51.010	55.600	0.000	0.209	51.01	55.809
	12	51.010	55.600	0.000	0.209	51.01	55.809
First-pass RO high-pressure pumps	13a	28.511	29.800	0.001	0.098	28.51	29.898
	13c	28.663	30.000	0.001	0.099	28.66	30.099
	14a	59.057	60.400	0.001	0.098	59.06	60.498
	14c	48.039	49.400	0.001	0.099	48.04	49.499
First-pass RO	15a	14.214	15.200	0.671	0.133	14.88	15.333
	15c	14.481	15.500	0.664	0.128	15.14	15.628
	16a	13.009	13.400	0.496	0.510	13.50	13.910
	16c	9.201	9.500	0.517	0.521	9.72	10.021
	17a	5.013	5.400	0.496	0.510	5.51	5.910
	17c	4.856	5.200	0.516	0.521	5.37	5.721
RO tank inlet	18	34.689	37.100	1.682	0.329	36.37	37.429
RO tank outlet (Pumps inlet)	19	34.689	37.100	1.682	0.329	36.37	37.429
Primary pumps out (Caustic inlet)	20	50.209	52.600	1.682	0.329	51.89	52.929
Caustic treatment outlet	21	50.209	52.600	1.372	0.217	51.58	52.817
First-pass RO high-pressure pumps	22b	16.743	17.600	0.457	0.072	17.20	17.672
	22c	16.412	17.200	0.448	0.071	16.86	17.271
	22d	17.053	17.900	0.466	0.074	17.52	17.974
	23b	54.096	54.900	0.458	0.072	54.55	54.972
	23c	55.233	56.000	0.449	0.071	55.68	56.071

	23d	54.869	55.700	0.467	0.074	55.34	55.774
	24b	17.585	18.300	0.529	0.112	18.11	18.412
	24c	18.373	19.100	0.513	0.108	18.89	19.208
	24d	19.042	19.800	0.532	0.112	19.57	19.912
Second-pass RO	25b	6.160	6.300	0.010	0.000	6.17	6.300
	25c	6.823	6.900	0.012	0.000	6.83	6.900
	25d	6.600	6.700	0.013	0.000	6.61	6.700
	26b	1.457	1.600	0.009	0.000	1.47	1.600
	26c	1.542	1.700	0.012	0.000	1.55	1.700
	26d	1.628	1.700	0.013	0.000	1.64	1.700
	27b	18.891	19.600	0.544	0.115	19.44	19.715
	27c	17.995	18.700	0.524	0.111	18.52	18.811
	27d	18.164	18.900	0.523	0.110	18.69	19.010
EDI process	28b	12.914	13.600	0.500	0.108	13.41	13.708
	28c	12.934	13.600	0.500	0.108	13.43	13.708
	28d	12.854	13.500	0.497	0.108	13.35	13.608
	29b	1.100	1.200	0.050	0.009	1.15	1.209
	29c	0.700	0.700	0.029	0.005	0.73	0.705
	29d	0.743	0.800	0.032	0.005	0.77	0.805
	30b	12.415	13.100	0.509	0.110	12.92	13.210
	30c	11.872	12.500	0.487	0.105	12.36	12.605
Primary mixed bed ion exchange	30d	12.134	12.800	0.497	0.108	12.63	12.908
	31b	11.310	12.000	0.509	0.110	11.82	12.110
	31c	10.816	11.500	0.487	0.105	11.30	11.605
	31d	10.884	11.700	0.490	0.108	11.37	11.808
One-micron cartridge filters	32	32.640	34.600	1.493	0.323	34.13	34.923
	33	32.099	34.000	1.493	0.323	33.59	34.323
UPW tank inlet	34	26.868	28.500	1.249	0.270	28.12	28.770
Diverted flow to RO tanks	35	5.232	5.500	0.243	0.053	5.47	5.553

References

[1] P. Palenzuela, B. Ortega-delgado, D. Alarcón-padilla, "Comparative assessment of the annual electricity and water production by concentrating solar power and desalination plants: A case study," *Appl. Therm. Eng.*, 2020:177:15485.
https://doi.org/10.1016/j.applthermaleng.2020.115485.

[2] Z. Rahimi-Ahar, M. S. Hatamipour, "A perspective of thermal type desalination: Technology, current development and thermodynamics analysis," Encyclopedia of Life Support Systems (EOLSS). http://www.eolss.net/Eolss-sampleAllChapter.aspx, 2020.

[3] K. Yousuf, 2019. "Efforts on to meet future water demand," Available:Https://www.omanobserver.om/efforts-on-to-meet-future-water-demand/.

[4] T. M. A. Al Sajwani, "The desalination plants of Oman: past, present and future," *Desalination*, 1998:120:8–13.
https://doi.org/10.1016/S0011-9164(98)00201-X.

[5] Z. Rahimi-Ahar, M. S. Hatamipour, L. Rahimi Ahar, "Air Humidification-Dehumidification Process for Desalination: A review," *Prog. Energy Combust. Sci.*, 2020:80:100850.
https://doi.org/10.1016/j.pecs.2020.100850.

[6] O. N. Igobo, P. A. Davies, "Isothermal Organic Rankine Cycle (ORC) driving Reverse Osmosis (RO) Desalination: experimental investigation and case study using R245fa working fluid," *Appl. Therm. Eng.*, 2018:136:740–746.
https://doi.org/10.1016/j.applthermaleng.2018.02.056.

[7] M. A. Darwish, N. M. Al-najem, "Energy consumption by multi-stage flash and reverse osmosis desalters," *Appl. Therm. Eng.*, 2000:20:399–416.
https://doi.org/10.1016/S1359-4311(99)00032-0.

[8] S. Ahmadvand, B. Abbasi, B. Azarfar, M. Elhashimi, "Looking beyond energy efficiency: an applied review of

water desalination technologies and an introduction to capillary-driven desalination," *water*, 2019:11:696–726. https://doi.org/10.3390/w11040696.

[9] Z. Rahimi-Ahar, M. S. Hatamipour, Y. Ghalavand, A. Palizvan, "Comprehensive study on vacuum humidification-dehumidification (VHDH) desalination," *Appl. Therm. Eng.*, 2020:114944. https://doi.org/10.1016/j.applthermaleng.2020.114944.

[10] F. Cziesla, G. Tsatsaronis, *Exergy, energy system analysis and optimization. Strengths and limitations of exergy analysis*, *Inst. Energy Eng.*, Vol. I, Springer. 1999.

[11] F. Fitzsimons, B. Corcoran, P. Young, G. Foley, "Exergy analysis of water purification and desalination: A study of exergy model approaches," *Desalination*, 2015:359:212–224. https://doi.org/10.1016/j.desal.2014.12.033.

[12] Y. Cerci, "Exergy analysis of a reverse osmosis desalination plant in California," *Desalination*, 2002:142: 257–266. https://doi.org/10.1016/j.desal.2004.08.045.

[13] N. Kahraman, Y.A. Cengel, B. Wood, Y. Cerci, "Exergy analysis of a combined RO, NF, and EDR desalination plant," *Desalination*, 2004:171:217–232. https://doi.org/10.1016/j.desal.2004.05.006.

[14] A. Shekari Namin, H. Rostamzadeh, P. Nourani, "Thermodynamic and thermoeconomic analysis of three cascade power plants coupled with RO desalination unit, driven by a salinity-gradient solar pond," *Therm. Sci. Eng. Prog*, 18, 100562, 2020. https://doi.org/10.1016/j.tsep.2020.100562.

[15] A. Mohammadi, M. Mehrpooya, "Energy and exergy analyses of a combined desalination and CCHP system driven by geothermal energy," *Appl. Therm. Eng.*, 116, 685–694, 2017. https://doi.org/10.1016/j.applthermaleng.2017.01.114.

[16] S. Islam, I. Dincer, B.S. Yilbas, "Development of a novel solar-based integrated system for desalination with heat recovery," *Appl. Therm. Eng.*, 129, 1618–1633, 2018. https://doi.org/10.1016/j.applthermaleng.2017.09.028.

[17] H. Ishaq, I. Dincer, G. F. Naterer, "New trigeneration system integrated with desalination and industrial waste heat recovery for hydrogen production," *Appl. Therm. Eng.*, 142, 767–778, 2018. https://doi.org/10.1016/j.applthermaleng.2018.07.019.

[18] N. Bouzayani, N. Galanis, J. Orfi, "Thermodynamic analysis of combined electric power generation and water desalination plants," *Appl. Therm. Eng.*, 29, 624–633, 2009.

[19] A. Naseri, M. Bidi, M. H. Ahmadi, "Thermodynamic and exergy analysis of a hydrogen and permeate water production process by a solar-driven transcritical CO_2 power cycle with liquefied natural gas heat sink," *Renew. Energy*, 113, 1215–1228, 2017. https://doi.org/10.1016/j.renene.2017.06.082.

[20] M. Ameri, M. Seyd Eshaghi, "A novel configuration of reverse osmosis , humidification – dehumidification and flat plate collector: Modeling and exergy analysis," *Appl. Therm. Eng*, 103, 855–873, 2016. https://doi.org/10.1016/j.applthermaleng.2016.04.047.

[21] A. Grabowski, G. Zhang, H. Strathmann, G. Eigneberger, "The production of high purity water by continuous electrodeionization with bipolar membranes: influuence of the anion-exchange membrane permselectivity," *J. Membr. Sci.*, 281, 297–306, 2006. https://doi.org/10.1016/j.memsci.2006.03.044.

[22] H. Lee, Y. Jin, S. Hong, "Recent transitions in ultrapure water (UPW) technology: Rising role of reverse osmosis (RO)," *Desalination*, 399, 185–197, 2016. https://doi.org/10.1016/j.desal.2016.09.003.

[23] M. Zhan, H. Lee, Y. Jin, S. Hong, "Application of MFI-UF on an ultrapure water production system to monitor the stable performance of RO process," *Desalination*, 491, 114565, 2020. https://doi.org/10.1016/j.desal.2020.114565.

[24] Y. Jin, H. Lee, M. Zhan, S. Hong, "UV radiation pretreatment for reverse osmosis (RO) process in ultrapure water (UPW) production," *Desalination*, 439, 138–146, 2018. https://doi.org/10.1016/j.desal.2018.04.019.[25] J. Wood, J. Gifford, J. Arba, M. Show, "Production of ultrapure water by continuous electrodeionization," *Desalination*, 250, 973–976, 2010. https://doi.org/10.1016/j.desal.2009.09.084.

[26] K. G. Nayar, M. H. Sharqawy, L. D. Banchik, J. H. Leinhard, "Thermophysical properties of seawater: A review and new correlations that include pressure dependence," *Desalination*, 390, 1–24, 2016. https://doi.org/10.1016/j.desal.2016.02.024.

[27] K. S. Pitzer, "Thermodynamics of electrolytes. I. Theoretical basis and general equations," *J. Phys. Chem.*, 77, 268−277, 1973. https://doi.org/10.1021/j100621a026.

[28] T. J. Kotas, *The exergy method of thermal plant analysis*, *1st Ed.*, Anchor Brendon Ltd. 1997. 29] H. Hassan, M. S. Yousef, "An assessment of energy, exergy and CO_2 emissions of a solar desalination system under hot climate conditions," *Process Saf. Environ. Prot.*, 145, 157-171, 2021. https://doi.org/10.1016/j.psep.2020.